Cellular/Molecular

An Epilepsy Mutation in the Sodium Channel *SCN1A* That Decreases Channel Excitability

Arthur J. Barela,[1]* Salina P. Waddy,[2]* Jay G. Lickfett,[1] Jessica Hunter,[3] Aimee Anido,[3] Sandra L. Helmers,[2] Alan L. Goldin,[1] and Andrew Escayg[3]

[1]Department of Microbiology and Molecular Genetics, University of California at Irvine, Irvine, California 92697-4025, and Departments of [2]Neurology and [3]Human Genetics, Emory University School of Medicine, Emory University, Atlanta, Georgia 30322

Mutations in three voltage-gated sodium channel genes, *SCN1A*, *SCN2A*, and *SCN1B*, and two $GABA_A$ receptor subunit genes, *GABRG2* and *GABRD*, have been identified in families with generalized epilepsy with febrile seizures plus (GEFS+). A novel mutation, R859C, in the $Na_v1.1$ sodium channel was identified in a four-generation, 33-member Caucasian family with a clinical presentation consistent with GEFS+. The mutation neutralizes a positively charged arginine in the domain 2 S4 voltage sensor of the $Na_v1.1$ channel α subunit. This residue is conserved in mammalian sodium channels as well as in sodium channels from lower organisms. When the mutation was placed in the rat $Na_v1.1$ channel and expressed in *Xenopus* oocytes, the mutant channel displayed a positive shift in the voltage dependence of sodium channel activation, slower recovery from slow inactivation, and lower levels of current compared with the wild-type channel. Computational analysis suggests that neurons expressing the mutant channel have higher thresholds for firing a single action potential and for firing multiple action potentials, along with decreased repetitive firing. Therefore, this mutation should lead to decreased neuronal excitability, in contrast to most previous GEFS+ sodium channel mutations, which have changes predicted to increase neuronal firing.

Key words: **epilepsy; sodium channel; electrophysiology; mutation; GEFS+; SCN1A**

Introduction

Generalized epilepsy with febrile seizure plus (GEFS+) is a heterogeneous autosomal dominant disorder in which family members exhibit multiple epilepsy phenotypes including absence, myoclonic, generalized tonic-clonic or partial seizures, as well as febrile seizures. The febrile seizures associated with GEFS+ can persist beyond 6 years of age and phenotypically may be simple or complex (Scheffer and Berkovic, 1997). Recent studies have demonstrated a role for the involvement of three voltage-gated sodium channel genes, *SCN1A* (Escayg et al., 2000, 2001; Wallace et al., 2001a), *SCN1B* (Wallace et al., 1998; Audenaert et al., 2003), and *SCN2A* (Sugawara et al., 2001a), and the $GABA_A$ receptor genes *GABRG2* (Baulac et al., 2001; Wallace et al., 2001b) and *GABRD* (Dibbens et al., 2004) in the pathogenesis of GEFS+. Only a small number of GEFS+ mutations have been identified, of which *SCN1A* accounts for the largest proportion, with 15 mutations reported to date.

$Na_v1.1$ is a 260 kDa transmembrane protein with four homologous domains (D1 to D4) that comprises the pore-forming α subunit of a voltage-gated sodium channel. The α subunit is associated with one or more β subunits in different tissues. Each domain of the α subunit contains six transmembrane segments (S1 to S6). The S4 segment of each domain is responsible for conferring the voltage-gating properties of the channel. To date, 4 of the 15 *SCN1A* GEFS+ mutations have been located in S4 segments, confirming the importance of this domain in channel function.

SCN1A dysfunction is also the most frequent cause of severe myoclonic epilepsy of infancy (SMEI), a debilitating childhood disorder characterized by febrile and afebrile seizures, mental retardation, and ataxia (Claes et al., 2001; Mulley et al., 2005). Individuals with SMEI and GEFS+ have been observed in the same family, suggesting that these two disorders represent the ends of a phenotypic continuum that may reflect the degree of sodium channel dysfunction (Singh et al., 2001).

Electrophysiological data, based on the analysis of a small number of *SCN1A* mutations, have revealed a range of biophysical abnormalities including alterations in the voltage dependence of activation and inactivation, accelerated recovery from inactivation, increased persistent current, as well as loss of channel function. The continued identification and analysis of *SCN1A* mutations is an important step toward understanding the relationship between sodium channel dysfunction and epilepsy.

Materials and Methods

Subjects. The proband (V-1) of a five-generation Caucasian family (see Fig. 1) was referred for evaluation for intractable epilepsy. During his clinical evaluation, he and subject III-2, who accompanied him, identified multiple family members with a history of epilepsy and febrile sei-

Received July 19, 2005; revised Jan. 20, 2006; accepted Jan. 24, 2006.

This work was supported by grants from the National Institutes of Health (NIH) (NS48336 to A.L.G.; NS046484 to A.E.), The McKnight Endowment Fund for Neuroscience (34653 to A.L.G.), Citizens United for Research in Epilepsy (A.E.), the March of Dimes (5-FY02-250 to A.E.), and the Emory University Research Council (2002120 to A.E.). This work was also supported in part by Public Health Service Grant M01-RR00039 from the General Clinical Research Centers Program, NIH, National Center for Research Resources. We thank Annie Lee, Hai Nguyen, Karoni Dutt, and Eric Sung for helpful discussions during the course of this work and Brian Tanaka for excellent technical assistance. We thank the family for its participation.

*A.J.B. and S.P.W. contributed equally to this work.

Correspondence should be address to Andrew Escayg at the above address. E-mail: aescayg@genetics.emory.edu.

DOI:10.1523/JNEUROSCI.2977-05.2006

 0270-6474/06/262714-10$15.00/0

Table 1. Clinical features of affected family members

	Age (years)			Clinical results	
Affected individual	At onset of febrile seizures	At last febrile seizure	Type of afebrile seizures	EEG	MRI
I-2	None		ND	ND	ND
III-2	2	7	None	ND	ND
III-4	ND	ND	None	ND	ND
III-9	None		GTCS	ND	ND
IV-2	2	7	None	ND	ND
IV-3	0.5	7	GTCS	Normal	Normal
IV-5	ND	ND	GTCS	ND	ND
IV-6	1	12	None	ND	ND
IV-10	1	7	GTCS	Normal	Normal
IV-11	None		GTCS	Normal	Normal
V-1	0.5	0.5	GTCS	Generalized intermittent polymorphic delta slowing	No structural abnormality after anterior 2/3 callosotomy
V-3	3	6	None	ND	ND

ND, Not determined; GTCS, generalized tonic clonic seizures.

zures. All available family members were interviewed by telephone, and seizure/epilepsy histories were documented and corroborated by other family members (Table 1). Medical records, including magnetic resonance imaging (MRI) and electroencephalography (EEG), were reviewed by a board-certified neurologist and neuroradiologist. All participants were enrolled in the study with appropriate institutional informed consent.

Mutation detection. Blood samples were collected from eight family members, and DNA was extracted by standard methods. DNA from affected individuals III-2 and V-1 were used for the initial screening of four candidate genes, *SCN1A*, *SCN2A*, *SCN1B*, and *GABRG2*. Additional family members were used to determine cosegregation of putative mutations.

The coding exons and exon/intron boundaries of the candidate genes were PCR amplified from genomic DNA. PCR amplification was performed at 32 cycles of 1 min at 94°C, 45 s at 55°C, and 2 min at 72°C. To facilitate heteroduplex formation, the PCR products were denatured at 99°C for 10 min and then 68°C for 30 min. Samples were analyzed by conformation sensitive gel electrophoresis (CSGE) and visualized by ethidium bromide staining as described previously (Escayg et al., 2000). PCR products that generated mobility variants on the CSGE gel were reamplified, purified, and analyzed on an ABI 3100 automated sequencer (Applied Biosystems, Foster City, CA). We also amplified 135 controls (270 alleles) of Northern European and Russian ancestry from the Centre d'Etude du Polymorphisme Humain (CEPH) DNA collection.

Site-directed mutagenesis. A product containing the R859C mutation was constructed by generating two overlapping PCR products using standard conditions: primer pair 1: forward 1 (F1), GAGACGCAATAGCAGAACAAG, reverse 1 (R1), CAGTCGGAATGAACAGAGAACTG; primer pair 2: F2, CAGTTCTCTGTTCATTCCGACTG, R2, GATGTACTTTTCCACACTGCTG. The two PCR products were combined and reamplified using the outside primers F1 and R2 to generate a product of 1614 bp. This product was sequenced to ensure that no errors were introduced during PCR amplification. Restriction enzyme digestion with *Bbv*CI and *Mfe*I generated a 1358 bp product. To generate the mutagenized clone, the digested PCR product was ligated to the *Bbv*CI–*Mfe*I-digested wild-type $rNa_v1.1$ cDNA clone.

The R859C clone was grown in HB101 cells at 37°C. Sequence analysis of the 6 kb cDNA confirmed the presence of the R859C mutation and the absence of any unwanted substitutions.

Expression and electrophysiology. The R859C mutation was cloned into a cDNA clone encoding $rNa_v1.1$, the rat channel that is orthologous to the human channel encoded by the *SCN1A* gene. The human and rat orthologs are 98% identical in amino acid sequence. The electrophysiological properties of the channels were determined in the absence and presence of the $\beta1$ subunit by expression in *Xenopus* oocytes.

Wild-type or mutant sodium channel α subunit RNA was transcribed *in vitro* from *Not*I-linearized DNA templates using the T7 mMESSAGE mMACHINE kit (Ambion, Austin, TX). Stage V oocytes that were removed from adult female *Xenopus laevis* frogs were injected with between 1 and 200 pg of RNA to obtain current amplitudes between 1 and 5 μA, as described previously (Goldin, 1991). When the channels were coexpressed with the $\beta1$ subunit, a 1:10 molar ratio of α to $\beta1$ RNA was injected.

Sodium currents were recorded using an OC-725B two-electrode voltage clamp (Warner Instruments, Hamden, CT) at room temperature with a DigiData 1322A interface (Molecular Devices, Foster City, CA) and pClamp 8.0 software (Molecular Devices), as described previously (Patton and Goldin, 1991; Kontis et al., 1997). Currents were recorded in ND-96 solution (in mM: 96 NaCl, 2 KCl, 1.8 $CaCl_2$, 1 $MgCl_2$, and 5 HEPES, pH 7.5) in the absence and presence of 500 nM tetrodotoxin (TTX). Capacitive transients were eliminated by subtraction of TTX recorded currents.

The voltage dependence of activation was analyzed using a step protocol in which oocytes were depolarized for 60 ms from a holding potential of −100 mV to a range of potentials between −95 and +50 mV in 5 mV increments. Peak currents were plotted against voltage, and the reversal potentials were determined by fitting each *I–V* curve with the following equation:

$$I = [1 + exp(-0.03937 \times z \times (V - V_{1/2}))]^{-1} \times g \times (V - V_r),$$

where I is the current amplitude, z is the apparent gating charge, V is the potential of the given pulse, $V_{1/2}$ is the half-maximal voltage, g is a factor related to the number of open channels during the given pulse, and V_r is the reversal potential. Conductance was then calculated directly using the following equation:

$$G = I/(V - V_r),$$

where G is conductance and I, V, and V_r are as described above. The conductance values were normalized to the maximum conductance and plotted against voltage, and the resulting curves were fit with the following two-state Boltzmann equation:

$$G = 1/[1 + exp(-0.03937 \times z \times (V - V_{1/2}))],$$

where z is the apparent gating charge, V is the potential of the given pulse, and $V_{1/2}$ is the potential for half-maximal activation.

The voltage dependence of steady-state inactivation was determined using a two-step protocol in which a conditioning pulse was applied from a holding potential of −100 mV to a range of potentials between −100 and +15 mV in 5 mV increments for 500 ms, immediately followed by a test pulse to −5 mV for 14.5 ms. The peak current amplitudes during the subsequent test pulses were normalized to the peak current amplitude during the first test pulse, plotted against the potential of the conditioning pulse, and fit with the following two-state Boltzmann equation:

$$I = 1/[1 + exp((V - V_{1/2})/a)],$$

where I is equal to the test-pulse current amplitude, V is the potential of the conditioning pulse, $V_{1/2}$ is the voltage for half-maximal inactivation, and a is the slope factor.

The kinetics of fast inactivation was analyzed using the same protocol used to study the voltage dependence of activation. Inactivation time constants were determined using the Chebyshev method to fit each trace with the following double exponential equation:

$$I = A_{fast} \times exp[-(t - K)/\tau_{fast}] + A_{slow} \times exp[-(t - K)/\tau_{slow}] + C,$$

where I is the current, A_{fast} and A_{slow} are the relative proportions of current inactivating with the time constants τ_{fast} and τ_{slow}, K is the time shift, and C is the steady-state persistent current.

Recovery from inactivation was analyzed using three separate two-pulse protocols. Each protocol began with a conditioning depolarization from a holding potential of −100 to −5 mV for 50 ms, which inactivated >95% of the channels. This was followed by a decreasing recovery time interval at −100 mV and a test depolarization to −5 mV. The three protocols differed only in the maximum length of recovery time and the time interval by which the recovery period decreased: 25 ms maximum and 1 ms decrements in the short protocol, 200 ms maximum and 5 ms decrements in the intermediate protocol, and 3000 ms maximum and 100 ms decrements in the long protocol. Fractional recovery was calculated by dividing the maximum current amplitude during the test pulse by the maximum current amplitude of the corresponding conditioning pulse. The recovery data were fit with either the double exponential equation:

$$I = 1 - [A_1 \times exp(-t/\tau_1) + A_2 \times exp(-t/\tau_2)]$$

or the triple exponential equation:

$$I = 1 - [A_1 \times exp(-t/\tau_1) + A_2 \times exp(-t/\tau_2) + A_3 \times exp(-t/\tau_3)],$$

in which A_1, A_2, and A_3 are the relative percentages of current that recovered with the time constants τ_1, τ_2, and τ_3, and t is the recovery time.

Use dependence was analyzed at frequencies of 30 Hz using 17.5 ms depolarizations to −5 mV from a holding potential of −100 mV. The protocol was performed for 1.32 s, which was approximately twice as long as necessary for the current to reach an equilibrium value. Peak current amplitudes were normalized to the peak current amplitude during the first depolarization and plotted against depolarization number.

The voltage dependence of steady-state slow inactivation was determined using a two-step protocol in which a conditioning pulse was applied from a holding potential of −120 mV to a range of potentials between −115 and 0 mV in 5 mV increments for a period of 90 s. The conditioning pulse was immediately followed by a hyperpolarization to −120 mV for 20 ms to allow for recovery from fast inactivation and a subsequent test pulse to −5 mV for 17.5 ms to assess slow inactivation. The peak current amplitudes during the subsequent test pulses were normalized to the peak current amplitude during the first test pulse, plotted against the potential of the conditioning pulse, and fit with the two-state Boltzmann equation described previously for the voltage-dependence of fast inactivation.

The rate of entry into the slow inactivated state was analyzed using a two-step protocol with a variable length conditioning pulse followed by a test pulse. The conditioning potential of −10 mV was applied from a holding potential of −120 mV for a variable, nonlinear length of time beginning with 0 s and ending with 29 s. Variable nonlinear increments were used to collect more data during the first 10 s, at which time >80% of the channels entered into slow inactivation. The conditioning pulse was immediately followed by a hyperpolarization to −120 mV for 20 ms to allow for recovery from fast inactivation and a subsequent test pulse to −5 mV. The peak current amplitudes during the subsequent test pulses were normalized to the peak current amplitude during the first test pulse and plotted against the period of the conditioning pulse. The kinetics of slow inactivation data were fit with a double exponential equation as described previously for the kinetics of fast inactivation.

Recovery from slow inactivation was analyzed using a two-pulse protocol beginning with a conditioning depolarization from a holding potential of −120 to −5 mV for 60 s, which inactivated >95% of the channels. This was followed by a decreasing recovery time interval at −120 mV for a nonlinear range of recovery times between 0 and 100 s. The conditioning pulse was immediately followed by a hyperpolarization to −120 mV for 20 ms to allow for recovery from fast inactivation and a subsequent test pulse to −5 mV. Fractional recovery was calculated by dividing the maximum current amplitude during the test pulse by the average maximum current amplitude during three single-step depolarizations to −5 mV recorded before each recovery protocol and plotted against the length of the recovery interval. The recovery data were fit with a double exponential equation as described previously for recovery from fast inactivation.

Computational model. Hodgkin-Huxley conductance based models of spiking neurons were constructed using the NEURON simulation software (Hines and Carnevale, 1997). Single compartment models of neuronal soma were constructed, and sodium and delayed rectifier potassium channels were included as described previously (Spampanato et al., 2004a). The models included either wild-type $Na_v1.1$ or R859C mutant channels with voltage dependencies and kinetics of slow inactivation as characterized in this study. The fast inactivation kinetics were based on wild-type values used previously (Spampanato et al., 2004b). The description of kinetics used for all sodium channels represent those that were determined with coexpression of the β1 subunit. The kinetics of the delayed rectifier K^+ channels was the same as that used previously (Spampanato et al., 2004a).

Experimentally determined voltage-dependent activation was fit with the following equation:

$$m_\infty^3(V) = (1/(1 + \exp((-e \times z \times (V - V_{1/2}))/kT)))^3,$$

where e is elementary charge, k is Boltzmann's constant, T is absolute temperature, $V_{1/2}$ is the half-maximal activation voltage, and z is the apparent charge movement for steady-state activation (m_∞). The $V_{1/2}$ and z values for m_∞ were then used to model sodium current activation for wild-type channels as follows:

$$m_\infty(V)^{Na_v1.1} = 1/(1 + \exp(-0.03937 \times 4.7 \times (V + 27.4))).$$

The R859C mutation altered the steady-state activation, and this change was modeled as follows:

$$m_\infty(V)^{R859C} = 1/(1 + exp(-0.03937 \times 3.5 \times (V + 21.3))).$$

The steady-state fast inactivation and kinetics for both wild-type and mutant channels were described using the following equations:

$$h_\infty(V) = 1/(1 + exp((V + 41.9)/6.7))$$

and

$$\tau_h(V) = 23.12 \times exp(-0.5 \times ((V + 77.58)/43.92)^2).$$

Steady-state slow inactivation and kinetics for wild-type channels were described using the following equations:

$$s_\infty(V) = 1/(1 + exp((V + 46.0)/6.6))$$

and

$$\tau_s(V)^{Na_v1.1} = 1000 \times 140.4 \times \exp(-0.5 \times ((V + 71.3)/30.9)^2).$$

The mutation altered the kinetics of slow inactivation, and this change was modeled using the following:

$$\tau_s(V)^{R859C} = 1000 \times 190.2 \times exp(-0.5 \times ((V + 90.4)/38.9)^2).$$

The sodium currents were described with activation and fast and slow inactivation as

$$I_{Na} = g_{Na} \times (V - E_{Na}),$$

where $g_{Na} = g_{Na}{}^{max} m^3 \times h \times s$, E_{Na} = 50 mV, and $g_{Na}{}^{max}$ = 200 mS/cm^2.

Results

Genetic analysis

CSGE analysis of subjects III-2 and V-1 (Fig. 1) identified several PCR products with mobility variants. All PCR products from the four candidate genes that generated mobility variants on the

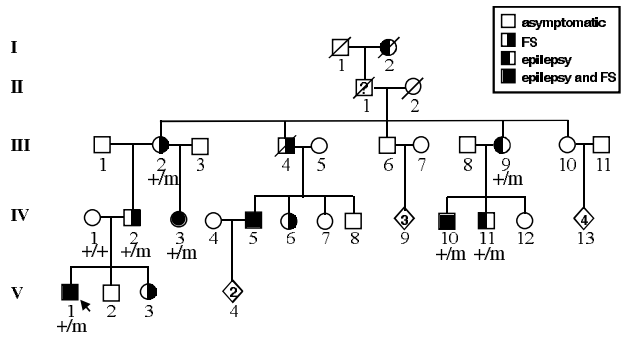

Figure 1. The R859C mutation cosegregates with disease in a large GEFS+ family. DNA was obtained from eight family members in three generations. Shading indicates diagnosis. +/m denotes individuals with mutation. +/+ denotes individuals without mutation. The arrow indicates the proband. FS, Febrile seizures.

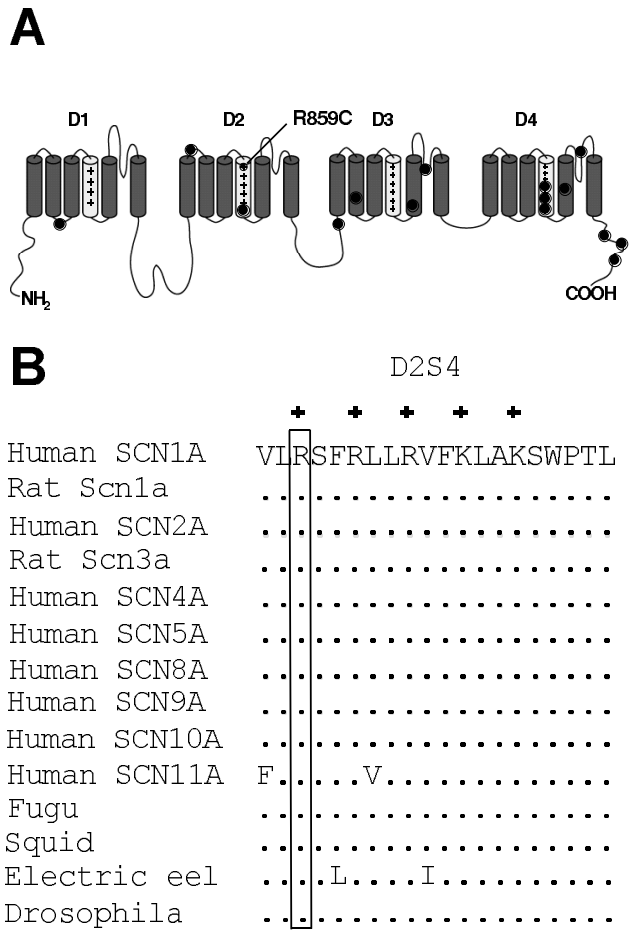

Figure 2. Location and conservation of R859C. ***A***, R859C results in the substitution of a positively charged arginine residue in the S4 segment of domain 2. Published GEFS+ mutations (filled circles) are distributed throughout SCN1A. ***B***, R859 is invariant in mammalian sodium channel genes and in sodium channels from lower organisms.

CSGE gel were sequenced. Sequence analysis of *SCN1A* exon 14 revealed the nucleotide substitution C2575T that resulted in the amino acid substitution R859C (Fig. 2*A*). R859 corresponds to the first arginine residue of the domain 2 S4 transmembrane segment. This amino acid residue is invariant in the mammalian sodium channels as well as in the sodium channels of lower organisms (Fig. 2*B*). With the exception of the R859C mutation, all other variants either were located within introns or were silent

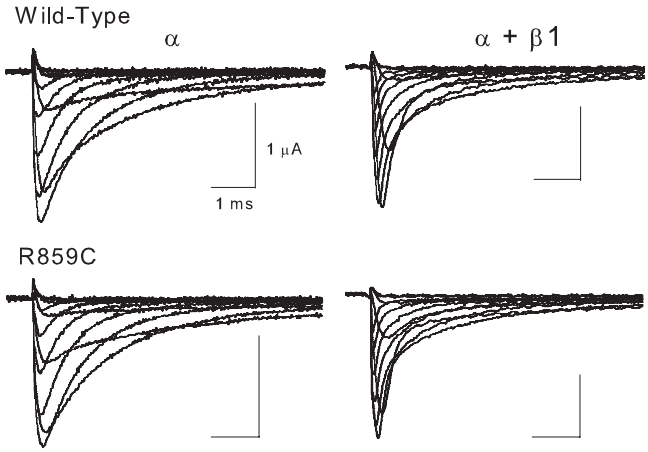

Figure 3. Currents through wild-type and R859C channels. Currents were recorded through the wild-type rNa$_v$1.1 and R859C channels expressed as α subunits alone and as α plus β1 subunits. Mutant and wild-type channels were expressed in *Xenopus* oocytes, and currents were recorded at 20°C using the two-electrode voltage clamp as described in Materials and Methods. Membrane depolarizations from a holding potential of −100 mV to a range of potentials from −50 to +50 mV in 10 mV increments are shown. Calibration: 1 ms, 1 μA.

substitutions in the coding exons and therefore were not considered to be disease-causing mutations. All available affected family members (III-9, IV-2, IV-3, IV-10, IV-11) were found to be heterozygous for the R859C mutation. R859C was not detected in 135 unrelated Northern European and Russian controls from the CEPH panel.

Electrophysiological analysis

To determine how the R859C mutation affects sodium channel function, we constructed the mutation in the orthologous rat channel rNav1.1, which is 98% identical in amino acid sequence to the human channel. The properties of the mutant channels were compared with those of wild-type channels expressed in *Xenopus* oocytes by using the two-electrode voltage clamp. The channels were compared in the absence and presence of the β1 subunit to determine whether the R859C mutation affected the interaction with β1, because mutations of β1 and mutations that affect the interaction of α and β1 are known to cause GEFS+ (Wallace et al., 1998, 2002; Spampanato et al., 2004b).

Figure 3 shows sample two-electrode voltage-clamp recordings of currents through wild-type and mutant channels during depolarizations between −50 and +50 mV in 10 mV increments. As can be seen, coexpression of the β1 subunit accelerated inactivation of the α subunit channels. There were no dramatic differences between the mutant and wild-type channels in either the presence or absence of β1.

R859C alters the voltage dependence of activation but not inactivation

Because R859C neutralizes a positive charge in one of the S4 voltage sensors, we hypothesized that it would alter the voltage dependence of channel gating. To test this prediction, we determined the voltage dependence of activation and fast inactivation. The voltage dependence of activation for the mutant channel (open circles) was shifted in the positive direction compared with that of the wild-type channel (black circles) when expressed as either the α subunit (Fig. 4*A*) alone or as α plus β1 subunits (Fig. 4*B*). The mutation caused a shift in the $V_{1/2}$ of activation to more positive potentials by ~8.5 mV in both the absence and presence of the β1 subunit (Table 2). In contrast, the voltage dependence of inactivation was not significantly different between the mutant

(open triangles) and wild-type (black triangles) channels when expressed as either the α subunit alone (Fig. 4*A*, Table 2) or as α plus β1 subunits (Fig. 4*B*, Table 2).

R859C does not alter the kinetics of fast inactivation

Because many different changes in sodium channel function can result in GEFS+ (Spampanato et al., 2001, 2003; Lossin et al., 2002, 2003), it was important to determine whether the R859C mutation had any additional effects on properties of the channel. We therefore quantitatively examined the kinetics of fast inactivation, although there were no obvious differences in the current traces shown in Figure 3. To quantify the kinetics, the current traces were fit with a double exponential equation, as described in Materials and Methods. The magnitudes of the fast (τ_{fast}, triangles) and slow (τ_{slow}, circles) time constants as well as the fractions of current that inactivated with τ_{fast} are shown in Figure 4, *C* and *D*. There were no significant differences in the magnitudes of the time constants when mutant and wild-type channels were expressed either as α subunits alone or as α plus β1 subunits. There were also no significant differences in the fractions of current that inactivated with τ_{fast} when mutant and wild-type channels were expressed in the absence or presence of the β1 subunit. Finally, the percentage of noninactivating (persistent) current was similar for both wild-type and mutant channels (data not shown).

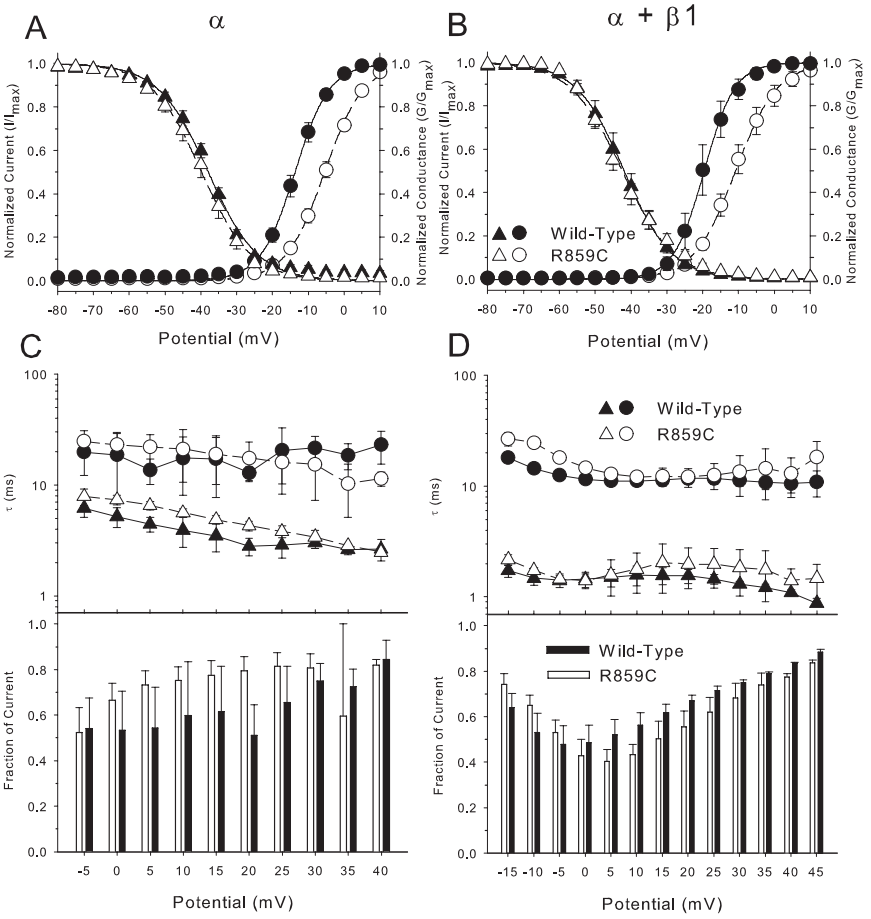

Figure 4. Voltage dependence and kinetics for wild-type and R859C channels. The voltage dependences of activation (circles) and inactivation (triangles) were determined for the wild-type $rNa_v1.1$ (filled symbols) and R859C (open symbols) channels expressed as α subunits alone (***A***) and as α plus β1 subunits (***B***). Sodium currents were recorded from a holding potential of −100 mV by depolarizations to a range of potentials from −95 to +50 mV in 5 mV increments. Normalized conductances were calculated by dividing the conductance at each potential by the maximum conductance, as described in Materials and Methods. The values shown are averages, and the error bars are SDs. The data were fit with a two-state Boltzmann equation, and the parameters of the fits are shown in Table 2. The voltage dependence of inactivation was determined using a two-step protocol in which a conditioning pulse was applied from a holding potential of −100 mV, consisting of 500 ms depolarizations to a range of potentials from −100 to +15 mV in 5 mV increments, followed by a test pulse to −5 mV. The peak current amplitude during each test pulse was normalized to the current amplitude of the first test pulse and plotted as a function of the conditioning pulse potential. The values shown are averages, and the error bars are SDs. The data were fit with a two-state Boltzmann equation, and the parameters of the fits are shown in the Table 2. The kinetics of inactivation was determined for wild-type $rNa_v1.1$ (filled symbols and bars) and R859C (open symbols and bars) channels by fitting the current traces with a double exponential equation as described in Materials and Methods. The time constants for the fast (τ_{fast}; triangles) and slow (τ_{slow}; circles) components of fast inactivation are plotted on a logarithmic scale in the top panels for α subunits alone (***C***) and α plus β1 subunits (***D***). The bottom panels indicate the fraction of current inactivating with τ_{fast}. In all cases, the sum of the components is one. The values shown are averages, and the error bars indicate SDs. Sample sizes were $rNa_v1.1$ α, 5; R859C α, 5; $rNa_v1.1$ α plus β1, 5; R859C α plus β1, 5.

R859C does not alter recovery from inactivation

Previous studies have shown that a GEFS+ mutation in $Na_v1.1$ can alter the kinetics of recovery from inactivation without affecting entry into the inactivated state (Spampanato et al., 2001). In addition, sodium channel mutations in $Na_v1.4$ and $Na_v1.5$ that alter recovery from inactivation cause paramyotonia congenita or ventricular fibrillation (Hayward et al., 1996; Chen et al., 1998). We therefore analyzed the effects of the R859C mutation on recovery from inactivation in the presence or absence of the β1 subunit, as described in Materials and Methods. Recovery from inactivation for the wild-type (filled circles) and R859C mutant (open circles) channels is shown in Figure 5*A* (α subunits alone) and Figure 5*B* (α plus β1 subunits), and the time constants for recovery are shown in Table 2. Coexpression of the β1 subunit accelerates recovery from inactivation, so that the data for α plus β1 subunits are best fit with two exponential time constants compared with three time constants for α subunits alone (Table 2). The R859C mutation increased the magnitude of the slowest time constant for α subunit channels (Table 2, τ_3), but this change had only a minimal effect on overall recovery (Fig. 5*A*). There were no significant differences in recovery for α plus β1 subunit channels (Fig. 5*B*, Table 2).

An alternative measure of recovery from inactivation is use dependence, in which the magnitude of the current is measured during a series of repetitive depolarizations. If there is insufficient time for recovery from inactivation between depolarizations, then the current decreases with successive pulses. Use dependence during depolarizations at 30 Hz was compared for the wild-type (filled circles) and R859C mutant (open circles) channels in Figure 5*C* (α subunits alone) and Figure 5*D* (α plus β1 subunits). Coexpression of the β1 subunit lessens the extent of use-dependent current decrease for both wild-type and mutant channels, but there were no significant differences between the

Table 2. Parameters of voltage dependence and recovery from inactivation

	Activation			Inactivation			Recovery from inactivation						
							τ_1		τ_2		τ_3		
Channel	$V_{1/2}$ (mV)	z (e_0)	n	$V_{1/2}$ (mV)	a (mV)	n	ms	%	ms	%	ms	%	n
WT	−13.7 ± 0.9	5.3 ± 0.2	5	−37.9 ± 0.9	6.9 ± 0.4	5	6.1 ± 2.8	12 ± 4	79 ± 32	46 ± 15	388 ± 149	41 ± 19	5
R859C	−5.4 ± 0.9*	4.7 ± 0.2*	5	−39.7 ± 1.4*	6.9 ± 0.4	5	6.9 ± 2.4	19 ± 9	128 ± 38	41 ± 13	613 ± 151*	38 ± 7	5
WT plus β1	−19.6 ± 1.9	6.0 ± 0.9	5	−41.9 ± 1.7	6.6 ± 0.4	5	2.6 ± 0.3	94 ± 5	104 ± 15	24 ± 5	ND[a]	ND[a]	5
R859C plus β1	−10.8 ± 1.5**	4.4 + 0.4**	5	−42.4 ± 1.4	7.2 ± 0.5	5	2.5 ± 0.3	96 ± 4	99 ± 10	23 ± 5	ND[a]	ND[a]	5
WT plus R859C+β1	−21.2 ± 3.1	5.1 ± 0.3**	6	ND[b]	ND[b]		ND[b]	ND[b]	ND[b]	ND[b]	ND[b]	ND[b]	

[a]Not determined because the recovery of these channels was best fit with a double exponential.

[b]Not determined because the inactivation and recovery from fast inactivation were not affected by the R859C mutation.

The asterisk indicates a statistically significant difference from wild-type (WT) α alone at $p < 0.05$; double asterisks indicate a statistically significant difference from WT α plus β1 at $p < 0.05$.

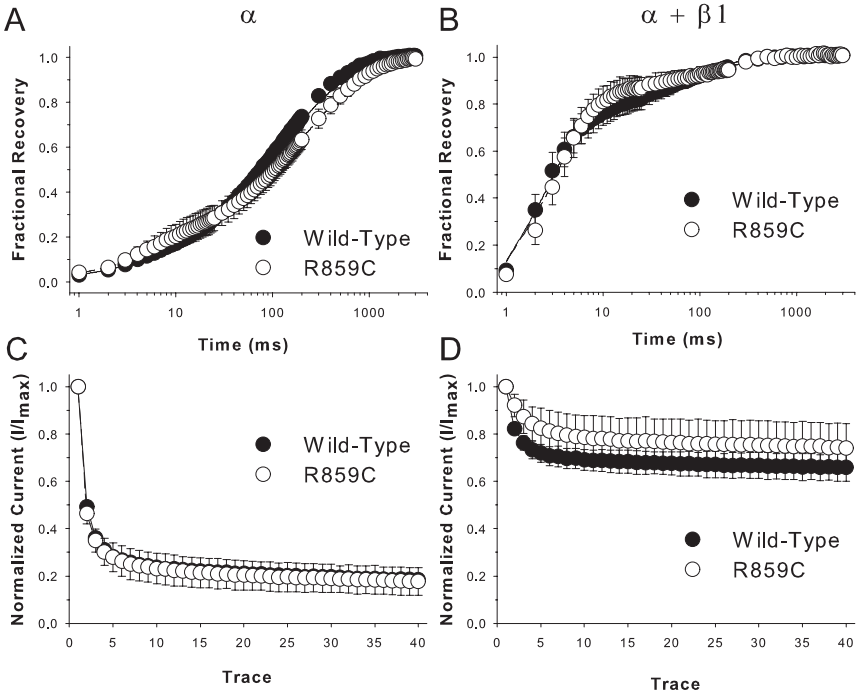

Figure 5. Recovery from inactivation and use dependence for wild-type and R859C mutant channels. Recovery from inactivation was determined using three separate, two-pulse protocols for wild-type rNa$_v$1.1 (filled symbols) and R859C (open symbols) channels. Each protocol was performed from a holding potential of −100 mV and consisted of a conditioning depolarization to −5 mV for 50 ms (which inactivated >95% of the channels), a decreasing recovery time interval at −100 mV, and a test depolarization to −5 mV. Fractional recovery was calculated by dividing the maximum current amplitude of the test pulse by the maximum current amplitude of the corresponding conditioning pulse. Fractional recovery is plotted on a log scale as a function of time for subunits alone (***A***) and α plus β1 subunits (***B***). The values shown are averages, and the error bars are SDs. Use dependence was analyzed at 30 Hz for wild-type rNa$_v$1.1 (filled symbols) and R859C (open symbols) channels. Currents were elicited using 17.5 ms depolarizations to −5 mV from a holding potential of −100 mV. Each protocol was performed until an equilibrium current had been reached (1.32 s). Peak current amplitudes were normalized to the initial peak current amplitude and plotted against pulse number for a subunits alone (***C***) and α plus β1 subunits (***D***). The values shown are averages, and the error bars are SDs. Sample sizes were rNa$_v$1.1 α, 5; R859C α, 5; rNa$_v$1.1 α plus β1, 5; R859C α plus β1, 5.

mutant and wild-type channels when expressed as either α subunits alone or as α plus β1 subunits.

R859C slows recovery from slow inactivation

In addition to the fast-gated properties examined above, some disease-causing mutations in the sodium channel, including at least one that causes GEFS+, alter slow inactivation (Cummins and Sigworth, 1996; Hayward et al., 1997; Bendahhou et al., 2000; Spampanato et al., 2001). Therefore, we examined the voltage dependence of slow inactivation, the rate of entry into the slow-inactivated state, and recovery from slow inactivation of R859C compared with wild-type α plus β1 subunit channels. We did not examine slow inactivation for channels consisting of the α subunit alone because it is difficult to distinguish slow from fast inactivation in those channels.

There were no significant differences in the voltage dependence of slow inactivation between R859C (open circles) and wild-type (black circles) channels (Fig. 6*A*, Table 3), nor were there any significant differences in entry into the slow inactivated state at −10 mV (Fig. 6*B*, Table 3). However, R859C channels recovered from slow inactivation significantly more slowly than did wild-type channels (Fig. 6*C*). The effect of the mutation was to increase the magnitude of τ_{slow} and to increase the fraction of current that recovered with τ_{slow} (Table 3).

Coexpression of R859C mutant with wild-type channels does not alter activation or recovery from slow inactivation

Because GEFS+ is an autosomal dominant disease (Scheffer and Berkovic, 1997; Singh et al., 1999), neurons in patients with GEFS+ express a heterogeneous mixture of wild-type and mutant channels. We therefore examined the effects of the R859C mutation in oocytes injected with similar amounts of wild-type and R859C RNA. To determine whether similar amounts of wild-type and R859C RNA express the same level of current, we injected 20 pg of wild-type or mutant RNA into *Xenopus* oocytes and measured the resulting currents after 24 h (α plus β1 subunits) or 48 h (α subunits). For α subunit channels, wild-type RNA expressed currents that were approximately twice the amplitude as those expressed from R859C RNA (Fig. 7*A*). For α plus β1 subunit channels, the difference was more pronounced, with wild-type RNA currents ~10-fold greater than R859C RNA currents (Fig. 7*A*).

To examine the effects of a mixed population of channels, oocytes were injected with equal quantities of wild-type and mutant RNA. Although the R859C mutation shifts the voltage dependence of activation in the positive direction (Fig. 4*A*,*B*), there was no change in the voltage dependence of activation when R859C RNA was coinjected with wild-type RNA in either the

absence (Fig. 7*B*) or presence (Fig. 7*C*) of the β1 subunit (Table 2). We also examined recovery from slow inactivation in oocytes coexpressing wild-type and R859C channels with β1, because the R859C mutation delayed recovery from slow inactivation (Fig. 6*C*). There was a slight increase in the slow time constant of recovery (Fig. 7*D*, Table 3), but this change did not significantly alter the overall recovery process. A likely explanation for the lack of effect on either the voltage dependence of activation or recovery from slow inactivation is that significantly less current was carried through R859C mutant compared with wild-type channels.

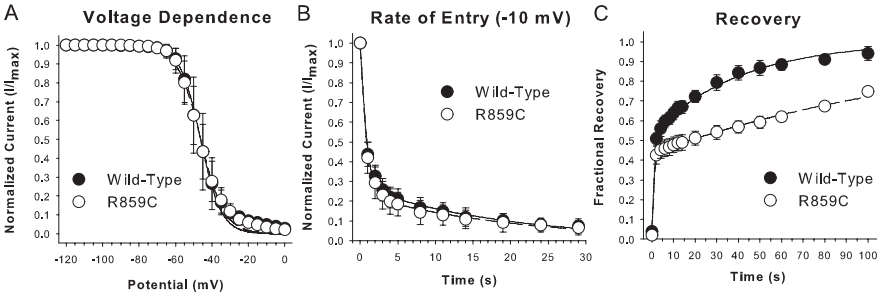

Figure 6. Slow-gated properties of wild-type and R859C channels. The slow-gated properties were determined for the wild-type rNa$_v$1.1 (filled circles) and R859C (open circles) channels expressed as α plus β1 subunits. ***A***, The voltage dependence of slow inactivation was analyzed using a two-step protocol in which a conditioning pulse was applied from a holding potential of −120 mV to potentials ranging from −115 to 0 mV in 5 mV increments for a period of 90 s. The conditioning pulse was immediately followed by a hyperpolarization to −120 mV for 20 ms to allow for recovery from fast inactivation and a subsequent test pulse to −5 mV for 17.5 ms to assess slow inactivation. The data were fit with a two-state Boltzmann equation as described in Materials and Methods, and the parameters of the fits and sample sizes are shown in Table 3. ***B***, The rate of entry into the slow inactivated state was analyzed using a two-step protocol with a variable length conditioning pulse followed by a test pulse. The conditioning potential of −10 mV was applied from a holding potential of −120 mV for times ranging from 0 to 29 s. The conditioning pulse was immediately followed by a hyperpolarization to −120 mV for 20 ms to allow for recovery from fast inactivation and a subsequent test pulse to −5 mV. The peak current amplitudes during the subsequent test pulses were normalized to the peak current amplitude during the first test pulse and plotted against the period of the conditioning pulse. The data were fit with a double exponential decay as described in Materials and Methods, and the parameters of the fits and the sample sizes are shown in Table 3. ***C***, Recovery from slow inactivation was analyzed using a two-pulse protocol beginning with a conditioning depolarization from a holding potential of −120 mV to −5 mV for 60 s, which inactivated >95% of the channels. This was followed by a decreasing recovery time interval at −120 mV for recovery times between 100 s and 0 s. The conditioning pulse was immediately followed by a hyperpolarization to −120 mV for 20 ms to allow for recovery from fast inactivation and a subsequent test pulse to −5 mV. Fractional recovery was calculated by dividing the maximum current amplitude during the test pulse by the average maximum current amplitude during three single-step depolarizations to −5 mV recorded before each recovery protocol and plotted against the length of the recovery interval. The data were fit with a double exponential equation as described in Materials and Methods, and the parameters of the fits and the sample sizes are shown in Table 3. For each graph, the values shown are averages, and the error bars are SDs.

R859C mutant channels produce a hypoexcitable model neuron

The R859C mutation shifted the voltage dependence of activation and delayed recovery from slow inactivation of the Na$_v$1.1 sodium channel. To determine how these changes might alter neuronal firing, we used a computational model based on the experimentally defined characteristics of the mutant sodium channels, as described previously (Spampanato et al., 2004a,b). The parameters of the wild-type and R859C mutant sodium channels differed in two aspects. First, the $V_{1/2}$ and z values for activation of the R859C channel were different from those of the wild-type channel (Table 2). Second, the kinetics of recovery from slow inactivation was delayed for the R859C mutant channel compared with that of the wild-type channel (Table 3). All other parameters were identical for mutant and wild-type channels.

The R859C mutation increased the threshold for firing action potentials, which was determined by injecting incrementally increasing amounts of current into a model neuron. A model neuron containing wild-type channels had a threshold for firing a single action potential of 140 pA (Fig. 8*A*). The R859C mutation increased this threshold to 150 pA (Fig. 8*B*), which was a direct result of the positive shift in the voltage dependence of activation. The mutation had a larger effect on the firing of multiple action potentials (Fig. 8*C*). Injection of ≥150 pA into a model neuron expressing wild-type channels resulted in the firing of multiple potentials, with a gradual increase as more current was injected. In contrast, a model neuron expressing R859C mutant channels required 160 pA to fire more than one action potential, and in that case, only two action potentials were observed. On the other hand, the rate of increase was rapid, so that the wild-type and mutant neurons fired similar numbers of action potentials when the amount of current injected was 170 pA or greater. We did not observe any differences in the frequency of repetitive discharges between neurons containing wild-type and mutant channels.

These results were obtained using model neurons expressing homogenous populations of either wild-type or mutant sodium channels. However, neurons in patients with GEFS+ express a heterogeneous mixture of wild-type and mutant channels. To determine the effects on neuronal firing of a mixed population, we varied the percentage of wild-type and mutant channels and determined the number of action potentials fired during injection of 150 pA of current (Fig. 8*D*). With this amount of current, a model neuron expressing all wild-type channels fired seven action potentials, whereas a model neuron with all mutant channels fired only one action potential. The number of action potentials changed dramatically as the ratio of wild-type to mutant channels decreased, so that a neuron with 50% mutant channels still fired five action potentials, whereas one with 60% mutant channels fired only a single action potential. Therefore, expression of a sufficient per-

Table 3. Parameters of slow inactivation

	Voltage dependence of slow inactivation			Entry into slow inactivation at −10 mV					Recovery from slow inactivation				
				τ_{fast}		τ_{slow}			τ_{fast}		τ_{slow}		
Channel	$V_{1/2}$ (mV)	a (mV)	n	s	%	s	%	n	s	%	s	%	n
WT plus β1	−46.2 ± 4.5	5.6 ± 0.8	12	0.79 ± 0.06	73 ± 8	19.6 ± 4.1	27 ± 8	5	0.85 ± 0.03	48 ± 3	40.5 ± 8.2	47 ± 4	6
R859C plus β1	−46.1 ± 3.8	6.4 ± 1.0	13	0.81 ± 0.07	77 ± 10	20.6 ± 1.2	23 ± 10	5	0.63 ± 0.1*	42 ± 4*	141.7 ± 10.2*	57 ± 4*	6
WT plus R859C plus β1	ND[a]	ND[a]		ND[a]	ND[a]	ND[a]	ND[a]		0.80 ± 0.13	56 ± 2*	59.7 ± 10.7*	39 ± 2*	4

[a]Not determined because the voltage dependence of slow inactivation and entry into slow inactivation were not affected by the R859C mutation.

The asterisk indicates a statistically significant difference from wild-type (WT) α plus β1 at $p < 0.05$.

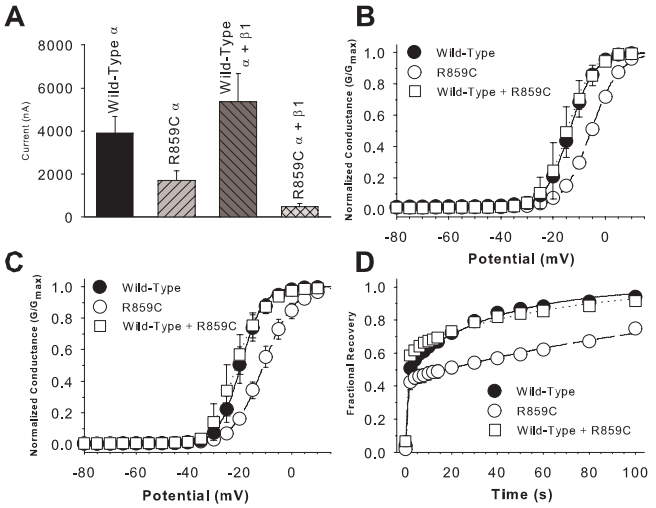

Figure 7. Expression of mixed populations of wild-type and R859C channels. ***A***, Mutant and wild-type channels were expressed in *Xenopus* oocytes by injection of 20 pg of RNA for either 24 h (α plus β1) or 48 h (α), after which sodium current amplitudes were measured during a depolarization to −5 mV from a holding potential of −100 mV. Sample sizes were wild-type α, 5; R859C α, 5; wild-type α plus β1, 5; R859C α plus β1, 5. ***B***, ***C***, The voltage dependence of activation was determined as described in the legend to Figure 4 for wild-type $rNa_v1.1$ (filled circles), R859C (open circles), and wild-type $rNa_v1.1$ plus R859C (open squares) in the absence (***B***) and presence (***C***) of the β1 subunit. The values shown are averages, and the error bars are SDs. The data were fit with a two-state Boltzmann equation, and the parameters of the fits and sample sizes are shown in Table 2. ***D***, Recovery from slow inactivation was determined as described in the legend to Figure 6 for the wild-type $rNa_v1.1$ plus β1 (filled circles), R859C plus β1 (open circles), and wild-type $rNa_v1.1$ plus R859C plus β1 (open squares). The data were fit with a double exponential equation as described in Materials and Methods, and the parameters of the fits and sample sizes are shown in Table 3. The values shown are averages, and the error bars are SDs.

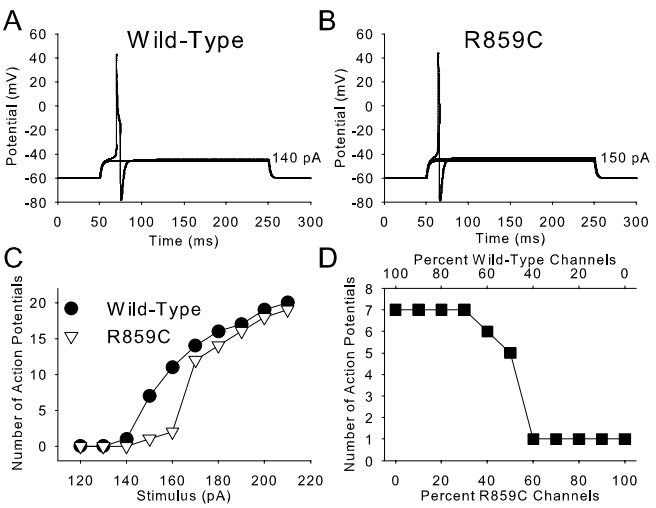

Figure 8. Computer simulation of neuronal firing. Action potential thresholds for model neurons with wild-type (***A***) or R859C (***B***) sodium channels are shown. Model neurons were injected with increasing amounts of current starting at 130 pA for a duration of 200 ms. The intensity of the stimulus was increased by 10 pA until a single action potential was observed. Steps shown correspond to 10 pA increments. ***C***, Model neurons with R859C mutant sodium channels fire fewer action potentials for a given stimulus compared with those with wild-type sodium channels. A current injection of 120 pA was applied to model neurons for a duration of 200 ms, and the number of action potentials was counted and plotted versus the stimulus intensity. This was repeated for increasing current injections in increments of 10 pA. ***D***, Model neurons were assigned a mixed population ranging from 0 to 100% mutant (100 to 0% wild-type) sodium channels, and the number of action potentials elicited during injection of 150 pA was determined and plotted versus the percentage of mutant channels.

centage of R859C mutant sodium channels greatly decreased repetitive neuronal firing.

Discussion

We have identified a novel *SCN1A* mutation that alters two aspects of sodium channel function, each of which was predicted to decrease neuronal firing. The clinical features of this family are similar to those of previously reported GEFS+ families in that the majority of affected family members have febrile seizures in isolation or in combination with other generalized seizures (9 of 12 members). Striking clinical variability was observed among the affected family members. The most severely affected family member, the proband (V-1), is cognitively impaired and has been refractory to multiple classes of anticonvulsant medications including those that inhibit voltage-gated sodium channels. This individual has undergone several surgical procedures including a corpus callosotomy and vagal nerve stimulation in an attempt to reduce seizure frequency. Other family members have had a more benign course resulting in resolution of the febrile seizures/generalized seizures or the seizures being controlled on medication. Subject II-1, an obligate carrier who was reported as unaffected and was unavailable for DNA analysis as a result of being deceased, may represent incomplete penetrance.

SCN1A is comprised of four homologous domains (D1 to D4), each of which has six transmembrane segments (S1 to S6) (Catterall, 2000). The fourth transmembrane segment (S4) of each domain contains conserved positively charged amino acids at intervals of 3, and these charged residues serve as the voltage sensors to initiate gating (Stühmer et al., 1991; Kontis et al., 1997; Mitrovic et al., 1998; Chanda et al., 2004). The R859C mutation neutralizes the first of five critical positively charged amino acids in the D2S4 of $Na_v1.1$. Neutralization of the comparable residue in other mammalian sodium channel isoforms shifts the voltage dependence of activation in the positive direction, with a 12.6 mV shift and a decrease in the slope in $Na_v1.2$ (Cestèle et al., 2001) and a 5.7 mV shift with a decrease in slope in $Na_v1.4$ (Mitrovic et al., 1998). A similar effect was observed in the bacterial sodium channel, in which the homologous mutation shifted the $V_{1/2}$ of activation by 12.6 mV in the positive direction (Chahine et al., 2004). Therefore, it is not surprising that the R859C mutation altered the voltage dependence of activation in $Na_v1.1$. This alteration in the voltage dependence of activation is predicted to increase the threshold for firing a single action potential (Spampanato et al., 2004a), which was observed in the computer model (Fig. 8*B*).

We also observed a significant decrease in the magnitude of current recorded after injection of the same quantity of R859C RNA compared with wild-type channel RNA (Fig. 7*A*). This result suggests that the mutation decreases expression of the channel, which would also be predicted to decrease neuronal excitability. The computer modeling of a mixed population of wild-type and mutant channels suggested that there was no effect of the R859C mutation on the number of action potentials until 40% of the channel population was mutant (Fig. 8*D*). That model assumed a constant number of channels in the cell, though, and a reduction in the total number of channels will also reduce action potential firing. Because expression levels in oocytes may not reflect expression levels in neuronal cells, we have not attempted to make any quantitative predictions based on the number of mutant versus wild-type channels.

In addition to the expected effect on the voltage dependence of activation, the R859C mutation significantly delayed recovery from slow inactivation (Fig. 6*C*, Table 3). The molecular mechanisms responsible for slow inactivation in sodium channels have

not been defined, but mutations in many different regions of the channel have been shown to affect the kinetics of slow inactivation (Cummins and Sigworth, 1996; Richmond et al., 1997; Mitrovic et al., 2000; Bendahhou et al., 2000; Alekov et al., 2001). However, it is unusual that the R859C mutation affected only recovery from slow inactivation, with no alterations in the kinetics of entry or the voltage dependence of slow inactivation. The slower recovery should result in decreased channel availability when the membrane is depolarized.

Both the positive shift in the voltage dependence of activation and the slower than normal recovery from slow inactivation are predicted to decrease neuronal excitability, although this prediction and the effects of the mutations need to be confirmed by expression in neurons because cell background can influence the physiological properties of the channels. This result is in contrast to the results for four previous *SCN1A* mutations that we examined by electrophysiological recording and computer modeling (T875M, W1204R, R1648H, D1866Y) (Spampanato et al., 2001, 2003, 2004a,b). Three of those mutations caused alterations that increased channel activity, whereas the fourth (T875M) enhanced slow inactivation (Spampanato et al., 2001, 2003, 2004b). However, all of the mutations were predicted to increase neuronal firing based on computer modeling (Spampanato et al., 2004a,b). Lossin et al. (2002) characterized three of the same mutations (T875M, W1204R, R1648H) and proposed that all three mutations cause epilepsy by increasing the percentage of persistent current. In addition, Cossette et al. (2003) demonstrated that sodium channels with the D188V mutation showed less of a decline in current amplitude during high-frequency depolarizations compared with wild-type channels. However, Lossin et al. (2003) also examined four other *SCN1A* mutations that decreased sodium channel activity (V1353L, I1656M, R1657C, and A1685V). I1656M and R1657C both caused 6–7 mV positive shifts in the voltage dependence of activation with no increase in persistent current, similar to our results for R859C, whereas V1353L and A1685V demonstrated no functional channel activity when transfected into tsA201 cells (Lossin et al., 2003). These results indicate that GEFS+ can be caused both by mutations that increase sodium channel activity as well as by those that decrease activity.

Most mutations that have been identified as causing GEFS+ are missense mutations in the *SCN1A* gene that are predicted to alter the biophysical properties of the $Na_v1.1$ sodium channel (Escayg et al., 2000, 2001; Abou-Khalil et al., 2001; Sugawara et al., 2001b; Wallace et al., 2001a; Lossin et al., 2002, 2003; Annesi et al., 2003; Fujiwara et al., 2003; Spampanato et al., 2004b). In contrast, most *SCN1A* mutations that have been identified in SMEI are predicted to result in null alleles or reduced protein levels (Claes et al., 2001, 2003; Sugawara et al., 2001b; Ohmori et al., 2002; Fujiwara et al., 2003; Nabbout et al., 2003; Wallace et al., 2003). The severity of clinical disorders resulting from mutations in *SCN1A* thus varies from mild to severe, with the most severe phenotype generally resulting from decreased sodium channel activity as in SMEI. The results with the R859C mutation, such as those of Lossin et al. (2003), demonstrate that decreased sodium channel activity can also cause a milder clinical phenotype typical for GEFS+.

The clinical characteristics of each GEFS+ family have shown that different *SCN1A* mutations may influence the clinical phenotype, severity, or response to established therapies. Different substitutions of the same amino acid residue can also dramatically alter phenotype and result in a clinical range from relatively benign (GEFS+) to severe (SMEI). For example, the *SCN1A* mutation R1648H was initially identified in a large GEFS+ family, whereas the *de novo* mutation R1648C was identified in an SMEI patient. Biophysical analyses of cloned *SCN1A* mutations have identified a range of altered channel properties that may underlie the epileptic phenotype. Continued analysis of the biophysical properties of mutant channels will provide insight into genotype/phenotype correlations and may eventually aid in the rational selection of therapeutic agents.

References

Abou-Khalil B, Ge Q, Desai R, Ryther R, Bazyk A, Bailey R, Haines JL, Sutcliffe JS, George Jr AL (2001) Partial and generalized epilepsy with febrile seizures plus and a novel *SCN1A* mutation. Neurology 57:2265–2272.

Alekov AK, Peter W, Mitrovic N, Lehmann-Horn F, Lerche H (2001) Two mutations in the IV/S4–S5 segment of the human skeletal muscle Na^+ channel disrupt fast and enhance slow inactivation. Neurosci Lett 306:173–176.

Annesi G, Gambardella A, Carrideo S, Incorpora G, Labate A, Pasqua AA, Civitelli D, Polizzi A, Annesi F, Spadafora P, Tarantino P, Cirò Candiano IC, Romeo N, De Marco EV, Ventura P, LePiane E, Zappia M, Aguglia U, Pavone L, Quattrone A (2003) Two novel SCN1A missense mutations in generalized epilepsy with febrile seizures plus. Epilepsia 44:1257–1258.

Audenaert D, Claes L, Ceulemans B, Löfgren A, Van Broeckhoven C, De Jonghe P (2003) A deletion in *SCN1B* is associated with febrile seizures and early-onset absence epilepsy. Neurology 61:854–856.

Baulac S, Huberfeld G, Gourfinkel-An I, Mitropoulou G, Beranger A, Prud'homme J-F, Baulac M, Brice A, Bruzzone R, LeGuern E (2001) First genetic evidence of $GABA_A$ receptor dysfunction in epilepsy: a mutation in the γ2-subunit gene. Nat Genet 28:46–48.

Bendahhou S, Cummins TR, Hahn AF, Langlois S, Waxman SG, Ptácek LJ (2000) A double mutation in families with periodic paralysis defines new aspects of sodium channel slow inactivation. J Clin Invest 106:431–438.

Catterall WA (2000) From ionic currents to molecular mechanisms: the structure and function of voltage-gated sodium channels. Neuron 26:13–25.

Cestèle S, Scheuer T, Mantegazza M, Rochat H, Catterall WA (2001) Neutralization of gating charges in domain II of the sodium channel a subunit enhances voltage-sensor trapping by a β-scorpion toxin. J Gen Physiol 118:291–301.

Chahine M, Pilote S, Pouliot V, Takami H, Sato C (2004) Role of arginine residue on the S4 segment of the *Bacillus halodurans* Na^+ channel in voltage-sensing. J Membr Biol 201:9–24.

Chanda B, Asamoah OK, Bezanilla F (2004) Coupling interactions between voltage sensors of the sodium channel as revealed by site-specific measurements. J Gen Physiol 123:217–230.

Chen Q, Kirsch GE, Zhang D, Brugada R, Brugada J, Brugada P, Potenza D, Moya A, Borggrefe M, Breithardt G, Ortiz-Lopez R, Wang Z, Antzelevitch C, O'Brien RE, Schulze-Bahr E, Keating MT, Towbin JA, Wang Q (1998) Genetic basis and molecular mechanism for idiopathic ventricular fibrillation. Nature 392:293–296.

Claes L, Del-Favero J, Cuelemans B, Lagae L, Van Broeckhoven C, De Jonghe P (2001) De novo mutations in the sodium-channel gene *SCN1A* cause severe myoclonic epilepsy of infancy. Am J Hum Genet 68:1327–1332.

Claes L, Ceulemans B, Audenaert D, Smets K, Löfgren A, Del-Favero J, Ala-Mello S, Basel-Vanagaite L, Plecko B, Raskin S, Thiry P, Wolf NI, Van Vroeckhoven C (2003) De novo *SCN1A* mutations are a major cause of severe myoclonic epilepsy of infancy. Hum Mutat 21:615–621.

Cossette P, Loukas A, Lafrenière RG, Rochefort D, Harvey-Girard E, Ragsdale DS, Dunn RJ, Rouleau GA (2003) Functional characterization of the D188V mutation in neuronal voltage-gated sodium channel causing generalized epilepsy with febrile seizures plus (GEFS). Epilepsy Res 53:107–117.

Cummins TR, Sigworth FJ (1996) Impaired slow inactivation in mutant sodium channels. Biophys J 71:227–236.

Dibbens LM, Feng H-J, Richards MC, Harkin LA, Hodgson BL, Scott D, Jenkins M, Petrou S, Sutherland GR, Scheffer IE, Berkovic SF, Macdonald RL, Mulley JC (2004) *GABRD* encoding a protein for extra- or perisynaptic $GABA_A$ receptors is a susceptibility locus for generalized epilepsies. Hum Mol Genet 13:1315–1319.

Escayg A, MacDonald BT, Meisler MH, Baulac S, Huberfeld G, An-Gourfinkel I, Brice A, LeGuern E, Moulard B, Chaigne D, Buresi C, Malafosse A (2000) Mutations of *SCN1A*, encoding a neuronal sodium channel, in two families with GEFS+2. Nat Genet 24:343–345.

Escayg A, Heils A, MacDonald BT, Haug K, Sander T, Meisler MH (2001) A novel *SCN1A* mutation associated with generalized epilepsy with febrile

seizures plus and prevalence of variants in patients with epilepsy. Am J Hum Genet 68:866–873.

Fujiwara T, Sugawara T, Mazaki-Miyazaki E, Takahashi Y, Fukushima K, Watanabe M, Hara K, Morikawa T, Yagi K, Yamakawa K, Inoue Y (2003) Mutations of sodium channel a subunit type 1 (SCN1A) in intractable childhood epilepsies with frequent generalized tonix-clonic seizures. Brain 126:531–546.

Goldin AL (1991) Expression of ion channels by injection of mRNA into *Xenopus* oocytes. Methods Cell Biol 36:487–509.

Hayward LJ, Brown Jr RH, Cannon SC (1996) Inactivation defects caused by myotonia-associated mutations in the sodium channel III-IV linker. J Gen Physiol 107:559–576.

Hayward LJ, Brown Jr RH, Cannon SC (1997) Slow inactivation differs among mutant Na channels associated with myotonia and periodic paralysis. Biophys J 72:1204–1219.

Hines ML, Carnevale NT (1997) The NEURON simulation environment. Neural Comput 9:1179–1209.

Kontis KJ, Rounaghi A, Goldin AL (1997) Sodium channel activation gating is affected by substitutions of voltage sensor positive charges in all four domains. J Gen Physiol 110:391–401.

Lossin C, Wang DW, Rhodes TH, Vanoye CG, George Jr AL (2002) Molecular basis of an inherited epilepsy. Neuron 34:877–884.

Lossin C, Rhodes TH, Desai RR, Vanoye CG, Wang D, Carniciu S, Devinsky O, George Jr AL (2003) Epilepsy-associated dysfunction in the voltage-gated neuronal sodium channel SCN1A. J Neurosci 23:11289–11295.

Mitrovic N, George Jr AL, Horn R (1998) Independent versus coupled inactivation in sodium channels. Role of the domain 2 S4 segment. J Gen Physiol 111:451–462.

Mitrovic N, George Jr AL, Horn R (2000) Role of domain 4 in sodium channel slow inactivation. J Gen Physiol 115:707–717.

Mulley JC, Scheffer IE, Petrou S, Dibbens LM, Berkovic SF, Harkin LA (2005) SCN1A mutations and epilepsy. Hum Mutat 25:535–542.

Nabbout R, Gennaro E, Dalla Bernardina B, Dulac O, Madia F, Bertini E, Capovilla G, Chiron C, Cristofori G, Elia M, Fontana E, Gaggero R, Granata T, Guerrini R, Loi M, La Selva L, Lispi ML, Matricardi A, Romeo A, Tzolas V, et al. (2003) Spectrum of *SCN1A* mutations in severe myoclonic epilepsy of infancy. Neurology 60:1961–1967.

Ohmori I, Ouchida M, Ohtsuka Y, Oka E, Shimizu K (2002) Significant correlation of the SCN1A mutations and severe myoclonic epilepsy in infancy. Biochem Biophys Res Commun 295:17–23.

Patton DE, Goldin AL (1991) A voltage-dependent gating transition induces use-dependent block by tetrodotoxin of rat IIA sodium channels expressed in *Xenopus* oocytes. Neuron 7:637–647.

Richmond JE, Featherstone DE, Ruben PC (1997) Human Na^+ channel fast and slow inactivation in paramyotonia congenita mutants expressed in *Xenopus laevis* oocytes. J Physiol (Lond) 499:589–600.

Scheffer IE, Berkovic SF (1997) Generalized epilepsy with febrile seizures plus. A genetic disorder with heterogeneous clinical phenotypes. Brain 120:479–490.

Singh R, Scheffer IE, Crossland K, Berkovic SF (1999) Generalized epilepsy with febrile seizures plus: a common childhood-onset genetic epilepsy syndrome. Ann Neurol 45:75–81.

Singh R, Andermann E, Whitehouse WPA, Harvey AS, Keene DL, Seni M-H, Crossland KM, Andermann F, Berkovic SF, Scheffer IE (2001) Severe myoclonic epilepsy of infancy: extended spectrum of GEFS$^+$. Epilepsia 42:837–844.

Spampanato J, Escayg A, Meisler MH, Goldin AL (2001) Functional effects of two voltage-gated sodium channel mutations that cause generalized epilepsy with febrile seizures plus type 2. J Neurosci 21:7481–7490.

Spampanato J, Escayg A, Meisler MH, Goldin AL (2003) The generalized epilepsy with febrile seizures plus type 2 mutation W1204R alters voltage-dependent gating of $Na_v1.1$ sodium channels. Neuroscience 116:37–48.

Spampanato J, Aradi I, Soltesz I, Goldin AL (2004a) Increased neuronal firing in computer simulations of sodium channel mutations that cause generalized epilepsy with febrile seizures plus. J Neurophysiol 91:2040–2050.

Spampanato J, Kearney JA, de Haan G, McEwen DP, Escayg A, Aradi I, MacDonald BT, Levin SI, Soltesz I, Benna P, Montalenti E, Isom LL, Goldin AL, Meisler MH (2004b) A novel epilepsy mutation in the sodium channel *SCN1A* identifies a cytoplasmic domain for β subunit interaction. J Neurosci 24:10022–10034.

Stühmer W, Conti F, Stocker M, Pongs O, Heinemann SH (1991) Gating currents of inactivating and non-inactivating potassium channels expressed in *Xenopus* oocytes. Pflügers Arch 418:423–429.

Sugawara T, Tsurubuchi Y, Agarwala KL, Ito M, Fukuma G, Mazaki-Miyazaki E, Nagafuji H, Noda M, Imoto K, Wada K, Mitsudome A, Kaneko S, Montal M, Nagata K, Hirose S, Yamakawa K (2001a) A missense mutation of the Na+ channel aII subunit gene *Nav1.2* in a patient with febrile and afebrile seizures causes channel dysfunction. Proc Natl Acad Sci USA 98:6384–6389.

Sugawara T, Mazaki-Miyazaki E, Ito M, Nagafuji H, Fukuma G, Mitsudome A, Wada K, Kaneko S, Hirose S, Yamakawa K (2001b) Nav1.1 mutations cause febrile seizures associated with afebrile partial seizures. Neurology 57:703–705.

Wallace RH, Wang DW, Singh R, Scheffer IE, George Jr AL, Phillips HA, Saar K, Reis A, Johnson EW, Sutherland GR, Berkovic SF, Mulley JC (1998) Febrile seizures and generalized epilepsy associated with a mutation in the Na^+-channel β1 subunit gene. SCN1B. Nat Genet 19:366–370.

Wallace RH, Scheffer IE, Barnett S, Richards M, Dibbens L, Desai RR, Lerman-Sadie T, Lev D, Mazarib A, Brand N, Ben-Zeev B, Goikhman I, Singh R, Kremmidiotis G, Gardner A, Sutherland GR, George Jr AL, Mulley JC, Berkovic SF (2001a) Neuronal sodium-channel α1-subunit mutations in generalized epilepsy with febrile seizures plus. Am J Hum Genet 68:859–865.

Wallace RH, Marini C, Petrou S, Harkin LA, Bowser DN, Panchal RG, Williams DA, Sutherland GR, Mulley JC, Scheffer IE, Berkovic SF (2001b) Mutant $GABA_A$ receptor γ2-subunit in childhood absence epilepsy and febrile seizures. Nat Genet 28:49–52.

Wallace RH, Scheffer IE, Parasivam G, Barnett S, Wallace GB, Sutherland GR, Berkovic SF, Mulley JC (2002) Generalized epilepsy with febrile seizures plus: mutation of the sodium channel subunit. SCN1B. Neurology 58:1426–1429.

Wallace RH, Hodgson BL, Grinton BE, Gardiner RM, Robinson R, Rodriguez-Casero V, Sadleir L, Morgan J, Harkin LA, Dibbens LM, Yamamoto T, Andermann E, Mulley JC, Berkovic SF, Scheffer IE (2003) Sodium channel α1-subunit mutations in severe myoclonic epilepsy of infancy and infantile spasms. Neurology 61:765–769.